DETC2022-90948

ON THE COMBINATION OF GEOMETRICALLY NONLINEAR MODELS AND SUBSTRUCTURING FOR MULTIBODY SIMULATION OF WIND TURBINE BLADES

Christian Sigurd L. Jensen, Rasmus B. E. Pedersen, Blas Blanco, José L. Escalona, Ole Balling[*]
Department of Mechanical and Production Engineering
Aarhus University, Denmark

ABSTRACT

This study develops a geometrically nonlinear model of a wind turbine blade utilizing finite strain theory for the calculation of elastic forces. The model is based on the floating frame of reference (FFR) formulation, which is a common choice in the modeling of long and flexible wind turbine blades. To model the nonlinear deformation of blades, the FFR formulation divides the structure into several substructures, which involves a significant increase of the system degrees of freedom. In the presented model, a nonlinear description of the elastic forces is introduced to achieve the convergence of the dynamic blade model at a lower number of substructures. The nonlinear elastic forces are formulated according to the Euler-Bernoulli beam theory, and they account for third-order terms of the potential elastic energy, the so-called geometric stiffness. The developed blade model is formulated in two dimensions and tested in a blade of 44.8 m length, which corresponds to a 2.75 MW wind turbine. Firstly, the results show that linear models do not accurately represent tip blade transverse displacement, and the substructuring technique becomes necessary to account for geometric nonlinearity. Secondly, using nonlinear elastic models significantly reduces the number of substructures needed to achieve convergence of the solution.

Keywords: Nonlinear phenomena, Structural dynamics, Wind energy, Rigid- and flexible-body dynamics

---

*Address all correspondence to this author at oba@mpe.au.dk.

1 Introduction

Wind turbine blades have features that make their modeling a complex task. Firstly, they undergo large displacements and rotations during working operations, which leads to nonlinear deformation of the blade. Secondly, the section is nonhomogeneous along its length and is made of composite material. Thirdly, the blade shape is pre-bent and pre-twisted to enhance the aeroelastic interaction during operation. Finally, they are subjected to complex loading scenarios due to wind.

Several methodologies can be used to meet these modeling requirements. For instance, OpenFast [1] software developed by NREL (National Renewable Energy Laboratory) implements BeamDyn [2], which uses geometrically exact beam theory based on the Legendre spectral Finite Element method. The software BHawC is an in-house code developed by the wind energy company Siemens-Gamesa, which uses a co-rotational formulation [3]. The Technical University of Denmark (DTU) and the certification company, DNV, have also developed their codes, HAWC2 [4] and Bladed [5], respectively, both based on the floating frame of reference (FFR) [6]. These models have the capability of formulating blade models capturing geometric nonlinearities.

Since blades have been continuously increasing in size and slenderness during the last decades, many researchers have paid attention to the potential effect of geometric nonlinearity on wind turbines performance. Manolas et al. [7] concluded that linear models are still acceptable in 5MW wind turbines (with blade lengths between 60 and 65 m), and around that value, nonlinear models become necessary. However, Wu et al. [8] obtained clear

different results between linear and non-linear models in a 5 MW blade. Moreover, centrifugal stiffening Burton et al. [**?**] predicted a significant centrifugal stiffening of a 40 m blade corresponding to a 2 MW wind turbine. Newly projected wind turbines reach 15 MW, with blade lengths about 117 m [9]. Therefore, the models intended to predict the response of new blades should pay special attention to geometrical nonlinear effects.

The FFR formulation used in Bladed and HAWC2 can account for geometric nonlinearity by introducing substructuring of the bodies [10]. However, the use of substructures increases the number of system degrees of freedom (DoF) and constraints. Therefore, an optimum number of substructures should be chosen to retain the geometric nonlinear effects while keeping the computational cost as low as possible. Moreover, the assessment of a blade model requires the simulation of a large number of load cases, and therefore the computational cost becomes an issue of utmost importance. Gözcü and Verelst [11] studied the minimum number of substructures required to capture nonlinear phenomena in the IEA (International Energy Agency) [12] and DTU (Technical University of Denmark) [13] reference 10 MW wind turbines. They conclude that 15 substructures are necessary to reach the problem convergence.

Geometric nonlinearities can be also accounted for in FFR formulation by introducing a nonlinear definition of the elastic force. Bakr and Shabana [14] propose a methodology to include nonlinear elastic forces resulting from some of the third-order terms of the potential elastic energy. The results are tested in a slider-crank mechanism. Later, Mayo et al. [15] defines a FFR formulation including all nonlinear forces due to third and fourth-order terms of the potential elastic energy. Finally, the performance of substructuring, nonlinear elastic modelling, together with the absolute nodal coordinate formulation is compared by Mayo et al. [16] for the case of the rotating beam introduced by Wu and Haug [10].

This study assesses the potential benefit of combining both substructuring and nonlinear elastic forces. In this way, it might be possible to achieve an accurate description of the nonlinear blade dynamics with a lower number of substructures, and therefore a lower number of DoF. The nonlinear elastic force definition accounts for the bending-stretching coupling and retains some of the third-order nonlinear terms in the strain-energy. The proposed methodology is tested in a 44.8 m long blade from a 2.75 MW wind turbine. The model is limited to a planar case using Euler-Bernoulli theory and does not account for other coupling phenomena like bending-twist. Initial configurations where the blade is pre-bent or pre-twisted are not considered. Loading conditions are approximated by including gravitational loads and a rotational driving constraint, which ramps up the rotational motion to the nominal angular velocity of the wind turbine. The results show that a single substructure with a linear elastic model is not appropriate for modeling a wind turbine blade. To achieve the convergence of the blade transverse tip displacement, about

10 substructures using linear elastic forces are necessary. However, the blade model using 4 substructures achieves convergence when nonlinear elastic forces are introduced.

2 Multibody formulation

The multibody formulation applied in this study to model the flexibility of the wind turbine blade is based on the FFR formulation further developed by Shabana [6]. Flexibility is introduced in the multibody formulation using the Finite Element (FE) Method based on prismatic Euler-Bernoulli beam elements. A substructuring technique is implemented in the multibody formulation, which divides the elastic body into a finite number of substructures.

2.1 Generalized coordinates

The generalized coordinates, $\mathbf{q}^i$, for an flexible body i used in a multibody dynamic system consists of reference and elastic coordinates, $\mathbf{q}_r^i$ and $\mathbf{q}_f^i$, respectively. Moreover, $\mathbf{q}_r^i$ can be partitioned into translational coordinates, $\mathbf{R}^i$, in a Cartesian coordinates system and rotational coordinates, $\mathbf{\Theta}^i$. The vector of generalized coordinates reads

$$\mathbf{q}^i = \begin{bmatrix} \mathbf{q}_r^i \\ \mathbf{q}_f^i \end{bmatrix} = \begin{bmatrix} \mathbf{R}^i \\ \mathbf{\Theta}^i \\ \mathbf{q}_f^i \end{bmatrix}. \tag{1}$$

In a two-dimensional case $\mathbf{q}_r^i$ can be described by two translational coordinates, x^i and y^i, and one rotational coordinate, θ^i, such that $\mathbf{q}_r^i = \begin{bmatrix} x^i & y^i & \theta^i \end{bmatrix}^T$. Regarding $\mathbf{q}_f^i$, it is an n-dimensional vector, in which the choice of a finite set of elastic coordinates is based on the Rayleigh-Ritz assumption.

The global position vector $\mathbf{r}_P^i$ of an arbitrary point P within the flexible body i is defined as

$$\mathbf{r}_P^i = \mathbf{R}^i + \mathbf{A}^i \bar{\mathbf{u}}^i, \tag{2}$$

where $\mathbf{R}^i$ denotes the global position of the body frame, $\mathbf{A}^i$ is transformation matrix between the i-th body frame and the global frame, and $\bar{\mathbf{u}}^i$ defines the position of the arbitrary point in the body frame, which can be defined by rigid and flexible contribution, $\bar{\mathbf{u}}_o^i$ and $\bar{\mathbf{u}}_f^i$, respectively, as shown in Fig. 1. The operator $(\bar{\ })$ denotes that the vector is defined in a body frame Therefore, Eqn. (2) becomes

$$\mathbf{r}_P^i = \mathbf{R}^i + \mathbf{A}^i \left(\bar{\mathbf{u}}_o^i + \bar{\mathbf{u}}_f^i \right), \tag{3}$$

where the flexible contribution is determined by utilizing the

Rayleigh-Ritz assumption as

$$\bar{\mathbf{u}}_f^i = \bar{\mathbf{S}}^i \bar{\mathbf{q}}_f^i, \tag{4}$$

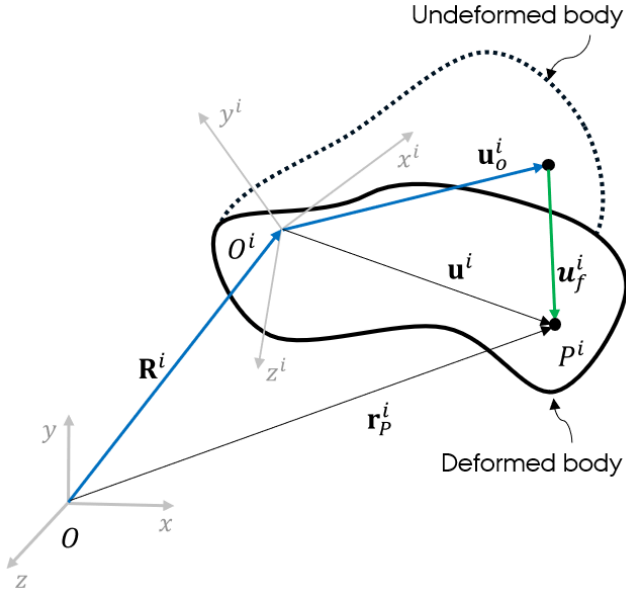being $\mathbf{S}^i$ the space-dependent shape function matrix.

FIGURE 1. Global description of arbitrary point P in flexible body i applying reference and flexible coordinates

2.2 Equations of motion

The equations of motion are written using the Lagrange multipliers technique, yielding:

$$\mathbf{M}\ddot{\mathbf{q}} + \mathbf{C}_{\mathbf{q}}^T \boldsymbol{\lambda} = \mathbf{Q}_e + \mathbf{Q}_v + \mathbf{Q}_{elas} + \mathbf{Q}_{damp}, \tag{5}$$

where $\mathbf{M}$ is the mass matrix, $\mathbf{C}_{\mathbf{q}}$ is the Jacobian of the constraint equations, $\boldsymbol{\lambda}$ contains the Lagrange multipliers and $\mathbf{Q}_e$, $\mathbf{Q}_v$, $\mathbf{Q}_{elas}$ and $\mathbf{Q}_{damp}$, are the vectors including the external, quadratic velocity, elastic and damping forces, respectively.

Equation (5) is augmented with the constraint equations at acceleration level as

$$\mathbf{C}_{\mathbf{q}}\ddot{\mathbf{q}} = -\dot{\mathbf{C}}_{\mathbf{q}}\dot{\mathbf{q}} - \dot{\mathbf{C}}_t, \tag{6}$$

which is solved by numerical integration. Baumgarte stabilization method is used to avoid the drift of the constraints.

2.3 Finite Element discretization

The flexible bodies are discretized by using FE. Subsequently, model order reduction is performed based on the eigenvalue problem. The FE mesh is also used to calculate the contribution of nonlinear forces. Euler-Bernoulli beam elements are utilized to assembly the mass and stiffness matrices of the body. The eigenvectors resulting from the eigenvalue analysis are the columns of the modal matrix, $\bar{\boldsymbol{\Phi}}$, that relates the nodal degrees of freedom belonging to the FE mesh, $\bar{\mathbf{n}}^i$, with the elastic coordinates as

$$\bar{\mathbf{n}}^i = \bar{\boldsymbol{\Phi}}^i \, \bar{\mathbf{q}}_f^i. \tag{7}$$

A reduced modal matrix, $\bar{\boldsymbol{\Phi}}_r^i$ is used to decrease the computational cost. The vibration modes from the modal matrix with the lowest associated natural frequencies are selected.

The shape function matrix used to describe the flexibility of element e that belongs to body i is now defined in terms of $\boldsymbol{\Phi}_r^i$ as

$$\bar{\mathbf{S}}^{ie} = \bar{\mathbf{A}}^e \bar{\mathbf{S}}^e \bar{\mathbf{A}}_6^e \bar{\mathbf{C}}^{ie} \bar{\mathbf{B}}^i \bar{\boldsymbol{\Phi}}_r^i, \tag{8}$$

where $\bar{\mathbf{A}}^e$ and $\bar{\mathbf{A}}_6^e$ define the transformation from element to global frame, $\bar{\mathbf{S}}^e$ is the FE shape function matrix, $\bar{\mathbf{C}}^{ie}$ is the connectivity matrix describing how the FE are connected and $\bar{\mathbf{B}}^i$ is a matrix that result from the boundary conditions of the FE mesh. The superscript e in the two transformation matrices denotes that they are element-dependent, which means that they are dependent on where along the discretized body the shape function matrix is evaluated. It is necessary to evaluate in which FE the point P lies at, in order to evaluate $\bar{\mathbf{S}}^e$ corresponding to that FE.

The slope of the midline of a bar-type flexible element e of body i is obtained as the spatial derivative of Eqn. (8), which leads to

$$\frac{\partial \bar{\mathbf{S}}^{ie}}{\partial \bar{x}^i} = \bar{\mathbf{A}}^e \frac{\partial \bar{\mathbf{S}}^e}{\partial \bar{x}^{ei}} \bar{\mathbf{A}}_6^e \bar{\mathbf{C}}^{ie} \bar{\mathbf{B}}^i \bar{\boldsymbol{\Phi}}_r^i, \tag{9}$$

where $\bar{x}^i$ and $\bar{x}^{ei}$ are the longitudinal coordinates in the i body frame and in the e element, belonging to the same body, respectively.

2.4 Substructuring

To capture geometrical nonlinearity using the FFR approach, the substructuring technique is utilized (Fig. 2). The method adds more generalized coordinates to the system since each substructure is described with its own body frame. Similarly, each substructure adds a set of new constraint equations. In turn, each substructure has its own FE mesh to determine the

corresponding modal shapes. For each body frame, a set of reference coordinates defines the position and orientation in space while a set of modal coordinates describes the deformation of the elements.
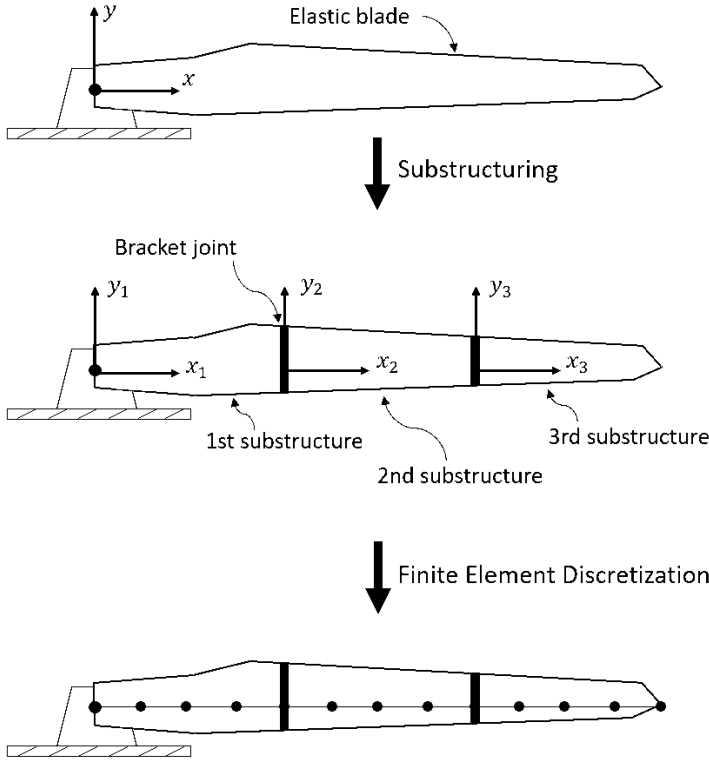

FIGURE 2. Flexible wind turbine blade divided into three substructures, where each substructure is discretized into a set of Finite Elements

The generalized coordinates of the substructures are related by translation and rotation compatibility conditions at each substructure interface. Fixed-free reference conditions are assumed for the substructures. Therefore, FE models use cantilever boundary conditions. The local reference frame is placed at the fixed end of each substructure. The implementation of the substructuring technique has been validated by recreating the results of a highly flexible spinning beam from the paper by Wu & Haug [10]. The disadvantage of this method is that the increased number of generalized coordinates and constraints lead to a decrease in computational efficiency.

To improve the computational efficiency of the substructuring technique, nonlinear beam FE could be used, since each element then will be able to describe accurately large displacements, which means that fewer substructures would be necessary to account for the geometric nonlinear behaviour of a wind turbine blade. Large deformation may occur even when strain is kept

small if components are large enough, as it is the case with a wind turbine blade. It can experience geometric nonlinearity and large displacements considering the small change in strain rate [10].

3 Elastic nonlinear model

The procedure for developing the linear and nonlinear elastic models is taken from the work of Mayo et al. [17].

3.1 Displacement field

The displacement field in a two-dimensional beam obeying Euler-Bernoulli theory reads

$$\bar{\mathbf{u}} = \begin{bmatrix} \bar{u} \\ \bar{v} \end{bmatrix} = \begin{bmatrix} \bar{u}_0 - \bar{y}\frac{\partial \bar{v}_0}{\partial \bar{x}} \\ \bar{v}_0 \end{bmatrix}, \quad (10)$$

where x and y are the longitudinal and transverse coordinates, respectively, $\bar{u}$ and $\bar{v}$ are the longitudinal and transverse displacements, respectively, and the subscript 0 refers to the value at $\bar{y} = 0$, the neutral axis.

3.2 Strain

The assumptions in infinitesimal strain theory are not valid when considering large deformations and therefore a strain model from finite strain theory must be used. The Green-Lagrange strain tensor [18, 19] reads

$$\bar{\varepsilon}_{ij} = \frac{1}{2}\left(\frac{\partial \bar{u}_i}{\partial \bar{x}_j} + \frac{\partial \bar{u}_j}{\partial \bar{x}_i} + \sum_{k=1}^{2}\frac{\partial \bar{u}_k}{\partial \bar{x}_i}\frac{\partial \bar{u}_k}{\partial \bar{x}_j}\right), \quad i,j = 1,2, \quad (11)$$

where subscript 1 and 2 refer to x and y directions, respectively. The axial strain ($\bar{\varepsilon}_{xx}$) is given by:

$$\bar{\varepsilon}_{xx} = \frac{\partial \bar{u}}{\partial \bar{x}} + \frac{1}{2}\left[\left(\frac{\partial \bar{u}}{\partial \bar{x}}\right)^2 + \left(\frac{\partial \bar{v}}{\partial \bar{x}}\right)^2\right]. \quad (12)$$

A simplification of the axial strain for the beam element is proposed by Sharf [20], where the first term inside the brackets is neglected since longitudinal deformation is expected to be negligible as compared with transverse deformation, simplifying Eqn. (12) to

$$\bar{\varepsilon}_{xx} \approx \frac{\partial \bar{u}}{\partial \bar{x}} + \frac{1}{2}\left(\frac{\partial \bar{v}}{\partial \bar{x}}\right)^2 = \bar{\varepsilon}_{xx}^l + \bar{\varepsilon}_{xx}^{nl}, \quad (13)$$

where $\bar{\varepsilon}xx^l$ ans $\bar{\varepsilon}_{xx}^{nl}$ are the linear and nonlinear axial strains, respectively. By using the definition of the displacement field in

Eqn. (10) both components of the strain yield

$$\bar{\varepsilon}_{xx}^l = \frac{\partial \bar{u}_0}{\partial \bar{x}} - \bar{y}\frac{\partial^2 \bar{v}_0}{\partial \bar{x}^2}, \tag{14}$$

$$\bar{\varepsilon}_{xx}^{nl} = \frac{1}{2}\left(\frac{\partial \bar{v}_0}{\partial \bar{x}}\right)^2. \tag{15}$$

3.3 Strain energy

For a linear elastic material that obeys Hooke's law, the strain energy for a beam-like body experiencing only axial strain reads

$$U = \frac{1}{2}\int_V \bar{\tau}_{xx}\bar{\varepsilon}_{xx}\mathrm{d}\bar{V}, \tag{16}$$

where τ_{xx} is the axial stress and V is the volume of the elastic body. Shearing strains have been neglected in this analysis, under the assumption that blades are rather slender structures, and their contribution to the strain energy has therefore been excluded. Nevertheless, this assumption is a subject of further confirmation. By using the constitutive relations, $\bar{\tau}_{xx} = E\bar{\varepsilon}_{xx}$, where E is the Young's modulus, along with Eqn. (13), the Eqn. (16) can be divided into three separate volume integrals

$$U = \frac{1}{2}\int_V E\left(\bar{\varepsilon}_{xx}^l\right)^2 \mathrm{d}\bar{V} + \int_V E\left(\bar{\varepsilon}_{xx}^l \bar{\varepsilon}_{xx}^{nl}\right)\mathrm{d}\bar{V}$$
$$+ \frac{1}{2}\int_V E\left(\bar{\varepsilon}_{xx}^{nl}\right)^2 \mathrm{d}\bar{V} = U_L + U_G + U_H. \tag{17}$$

The terms in the strain energy in Eqn. (17) are labelled as U_L, U_G and U_H, respectively. U_L retains all terms to develop the constant conventional linear stiffness matrix. U_G constitutes what is described as the geometric stiffness matrix and is dependent on the axial elastic coordinates of the body. With respect to U_H, a second-order nonlinear stiffness matrix can be developed [17]. The second-order nonlinear stiffness matrix is highly nonlinear and requires a large number of high-frequency axial modes. This is due to the axial deformation being affected both by axial forces, but also by the foreshortening effect due to bending [17]. Capturing accurately the foreshortening effect requires accounting for a large number of axial modes. It would increase significantly the computational cost of the simulation since they are related to high natural frequencies. Because of this reason, along with the fact that second-order nonlinearities are expected to have a reduced impact as compared with first-order nonlinearity, U_H is excluded from this analysis.

By using Eqn. (14) into U_L and after some mathematical treatment, it yields

$$U_L = \frac{1}{2}\left[\int_L EA\left(\frac{\partial \bar{u}_0}{\partial \bar{x}}\right)^2 \mathrm{d}\bar{x} + \int_L EI_z\left(\frac{\partial^2 \bar{v}_0}{\partial \bar{x}^2}\right)^2 \mathrm{d}\bar{x}\right], \tag{18}$$
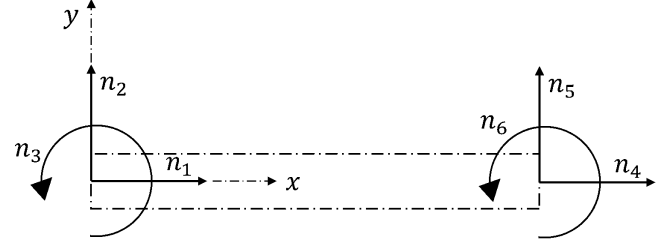

FIGURE 3. Two dimensional beam element

where L is the length of the beam, A is the cross-sectional area and I_z is the second moment of area. It should be noted that the area integral makes vanishing those terms proportional to $\bar{y}$.

The second part of the strain energy, U_G, can be expanded and treated in similar manner as U_L, yielding

$$U_G = \frac{1}{2}\int_V 2E\left[\left(\frac{\partial \bar{u}_0}{\partial \bar{x}} - \bar{y}\frac{\partial^2 \bar{v}_0}{\partial \bar{x}^2}\right)\frac{1}{2}\left(\frac{\partial \bar{v}_0}{\partial \bar{x}}\right)^2\right]\mathrm{d}\bar{V}$$
$$= \frac{1}{2}\int_L EA\left(\frac{\partial \bar{u}_0}{\partial \bar{x}}\right)\left(\frac{\partial \bar{v}_0}{\partial \bar{x}}\right)^2 \mathrm{d}\bar{x}, \tag{19}$$

in which again those terms proportional to $\bar{y}$ become zero after area integration.

3.4 Shape function matrix

The axial and lateral displacements of a point in the midline of a FE can be calculated as

$$\bar{\mathbf{u}}_0^e = \bar{\mathbf{S}}^e\left(\bar{\xi}\right)\bar{\mathbf{n}}^e = \begin{bmatrix} \bar{u}_0 & \bar{v}_0 \end{bmatrix}^T, \tag{20}$$

where $\bar{\xi} = \bar{x}/L$ and $\bar{\mathbf{n}}^e$, is the vector of nodal coordinates shown in Fig. 3. The FE shape function matrix reads

$$\bar{\mathbf{S}}^e\left(\bar{\xi}\right) = \begin{bmatrix} \bar{S}_1 & 0 & 0 & \bar{S}_4 & 0 & 0 \\ 0 & \bar{S}_2 & \bar{S}_3 & 0 & \bar{S}_5 & \bar{S}_6 \end{bmatrix} = \begin{bmatrix} \bar{\mathbf{S}}_x \\ \bar{\mathbf{S}}_y \end{bmatrix}, \tag{21}$$

where $\bar{\mathbf{S}}_x$ and $\bar{\mathbf{S}}_y$ contain the axial and transverse shape functions, respectively. The latter corresponds to the Euler-Bernoulli beam FE [6,21]. Their definition read

$$\begin{array}{ll}
\bar{S}_1 = 1 - \bar{\xi}, & \bar{S}_4 = \bar{\xi}, \\
\bar{S}_2 = 1 - 3(\bar{\xi})^2 + 2(\bar{\xi})^3, & \bar{S}_5 = 3(\bar{\xi})^2 - 2(\bar{\xi})^3, \\
\bar{S}_3 = l\left[\bar{\xi} - 2(\bar{\xi})^2 + (\bar{\xi})^3\right], & \bar{S}_6 = l\left[(\bar{\xi})^3 - (\bar{\xi})^2\right].
\end{array} \tag{22}$$

3.5 Stiffness matrices

The stiffness matrices of the FE are obtained by rewriting the definition of the potential elastic energy in terms of $\mathbf{u}_0^e$. In the case of Eqn. (18), it yields

$$U_L = \frac{1}{2}\int_L EA\left(\frac{\partial \bar{\mathbf{S}}_x}{\partial \bar{x}}\bar{\mathbf{n}}\right)^2 d\bar{x} + \frac{1}{2}\int_L EI_z\left(\frac{\partial^2 \bar{\mathbf{S}}_y}{\partial \bar{x}^2}\bar{\mathbf{n}}\right)^2 d\bar{x}, \quad (23)$$

which after rearranging becomes

$$U_L = \frac{1}{2}\bar{\mathbf{n}}^T\left[\int_L EA\left(\frac{\partial \bar{\mathbf{S}}_x}{\partial \bar{x}}\right)^T\left(\frac{\partial \bar{\mathbf{S}}_x}{\partial \bar{x}}\right)d\bar{x}\right]\bar{\mathbf{n}} + \\ \frac{1}{2}\bar{\mathbf{n}}^T\left[\int_L EI_z\left(\frac{\partial^2 \bar{\mathbf{S}}_y}{\partial \bar{x}^2}\right)^T\left(\frac{\partial^2 \bar{\mathbf{S}}_y}{\partial \bar{x}^2}\right)d\bar{x}\right]\bar{\mathbf{n}}. \quad (24)$$

It is then possible to insert the relevant partial derivatives of the shape function matrix and integrate the expressions separately. After rewriting Eqn. (24), the constant linear stiffness matrix, $\mathbf{K}_L$, arises as

$$U_L = \frac{1}{2}\bar{\mathbf{n}}^T\mathbf{K}_L\bar{\mathbf{n}}. \quad (25)$$

The matrix $\mathbf{K}_L$ can efficiently be obtained by utilizing the Symbolic Math Toolbox in *MATLAB*. The constant linear stiffness matrix ($\mathbf{K}_L$) for a beam element yields

$$\mathbf{K}_L = \frac{EI_z}{L}\begin{bmatrix} \frac{A}{I_z} & & & & & \\ 0 & \frac{12}{L^2} & & & sym. & \\ 0 & \frac{6}{L} & 4 & & & \\ -\frac{A}{I_z} & 0 & 0 & \frac{A}{I_z} & & \\ 0 & -\frac{12}{L^2} & -\frac{6}{L} & 0 & \frac{12}{L^2} & \\ 0 & \frac{6}{L} & 2 & 0 & -\frac{6}{L} & 4 \end{bmatrix}. \quad (26)$$

Castigliano's first theorem [21] states that if the strain energy is a function of the generalized displacements, then a generalized elastic force may be expressed as

$$\mathbf{Q}_{elas} = -\frac{\partial U}{\partial \bar{\mathbf{n}}}. \quad (27)$$

For the case of the linear elastic energy, applying Castigliano's first theorem to Eqn. (25) simply yields

$$\frac{\partial U_L}{\partial \bar{\mathbf{n}}} = -\mathbf{K}_L\bar{\mathbf{n}}. \quad (28)$$

Following a similar procedure for the second strain energy term (U_G), and noting that this term depends on the axial elastic coordinates it is possible to write

$$\frac{\partial U_G}{\partial \bar{\mathbf{n}}} = -\mathbf{K}_G\bar{\mathbf{n}} + \mathbf{Q}_G, \quad (29)$$

where $\mathbf{Q}_G$ is a nonconstant elemental vector of nonlinear elastic forces and $\mathbf{K}_G$ is the geometric stiffness matrix. Their definition read

$$\mathbf{Q}_G = -\frac{1}{2}\begin{bmatrix} \bar{\mathbf{n}}^T\left(\frac{\partial \mathbf{K}_G}{\partial \bar{n}_1}\right)\bar{\mathbf{n}} \\ \vdots \\ \bar{\mathbf{n}}^T\left(\frac{\partial \mathbf{K}_G}{\partial \bar{n}_6}\right)\bar{\mathbf{n}} \end{bmatrix}, \quad (30)$$

and

$$\mathbf{K}_G = \frac{EA\Delta\bar{u}}{L^2}\begin{bmatrix} 0 & & & & & \\ 0 & -\frac{6}{5} & & & sym. & \\ 0 & -\frac{L}{10} & -\frac{2L^2}{15} & & & \\ 0 & 0 & 0 & 0 & & \\ 0 & \frac{6}{5} & \frac{L}{10} & 0 & -\frac{6}{5} & \\ 0 & -\frac{L}{10} & \frac{L^2}{30} & 0 & \frac{L}{10} & -\frac{2L^2}{15} \end{bmatrix}, \quad (31)$$

where $\Delta\bar{u} = n_1 - n_4$ is the change in the axial elastic coordinates. This stiffness matrix adds the bending-stretch coupling since new bending stiffness terms are added, which are dependent on the axial deformations in the body.

After the development of the linear and non-linear FE stiffness matrices, it is possible to present the two elastic models used in the present analysis to model the generalized elastic forces. These elastic models will be named according to the paper by Mayo et al. [17] based on the order of terms introduced. The element force vector $\mathbf{Q}_G$ can be shown to contain second-order non-linear terms depending on the transverse and rotational coordinates. To keep this analysis on the influence of first-order non-linear terms, $\mathbf{Q}_G$ has not been included in this analysis. The linear formulation (L) is constant, whereas the nonlinear formulation (NL1) depends on the axial elastic coordinates and must be updated in a dynamic analysis. On an element basis these elastic models can be expressed as:

1. The linear formulation (L): $\quad \mathbf{K}_L\bar{\mathbf{n}}$.
2. The nonlinear formulation 1 (NL1): $\quad (\mathbf{K}_L + \mathbf{K}_G)\bar{\mathbf{n}}$.

4 Blade modelling

The wind turbine blade that has been modelled in the present study is based on the data presented in the PhD thesis of Holm-Jørgensen [22]. The blade is from a 2.75 MW wind turbine, and it has a length of 44.8 m and a weight of 9960 kg. Cross-sectional data is provided for 22 sections. In the multibody dynamics model developed, it is possible to divide the blade into substructures where each substructure has a unique set of beam FE with different cross-sectional properties. The blade is therefore modelled as non-prismatic as shown in Fig. 4. Gravitational effects are considered, but the effects arising from the offset between the local airfoil coordinate systems with respect to the center of gravity, for example, the elastic and shear centers, has not been included in the present study to keep as a two-dimensional problem. The blade is neither pre-bent nor pre-twisted in its initial configuration.
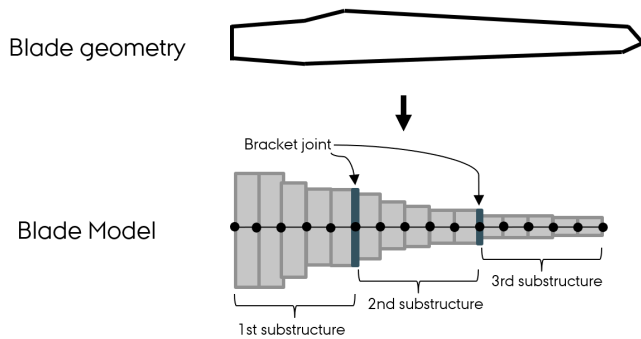
FIGURE 4. Nonprismatic blade model with variational cross-sectional area using three substructures

The blade can be considered slender, which means that shear deformation can be neglected. Based on the data from the blade provided by Holm-Jørgensen [22] the criterion for an Euler-Bernoulli assumption is assessed. The Euler-Bernoulli assumption is valid when κ is much smaller than 1

$$\kappa = \frac{12EI_z k_y}{AGL^2} \ll 1, \tag{32}$$

where k_y is the shear coefficient. According to Cook [23], k_y must be about 2 for a thin-walled circular cross-section, which is the case when the blade is examined at the blade root cross-section. For the case here studied $\kappa = 0.016$ at the blade base, and therefore the Euler-Bernoulli assumption is suitable for this problem. Dissipation is introduced as modal damping, where the damping ratio for all modes is kept constant at 0.01.

The dynamic response of the wind turbine blade is simulated using a rotational driving constraint with a time-dependent ramp-up function. A final angular velocity, ω, of 1.6 rad/s, which is

the nominal angular velocity of the 2.75 MW wind turbine, is reached after 15 seconds. However, the response of the blade will be simulated for additional 35 seconds to ensure that a steady-state response is obtained. The angular position of the rotating blade is prescribed by

$$\theta(t) = \begin{cases} \left(\frac{\omega}{T_s}\right)\left[\left(\frac{t^2}{2}\right) + \left(\frac{T_s}{2\pi}\right)^2 \left(\cos\left(\frac{2\pi t}{T_s}\right) - 1\right)\right], & 0 \le t < T_s \\ \omega\left(t - \frac{T_s}{2}\right), & T_s \le t \end{cases} \tag{33}$$

where T_s is a spin-up time and t is the total simulation time, set at 15 and 50 s, respectively. This ramp function is taken from the rotating beam problem used by Wu and Haug [10]. The wind load is not considered since the main goal is to assess differences between linear and non-linear modelling.

5 Numerical results

The flexible deformation of the blade due to rotation is interpreted in terms of the transverse and axial tip displacements. They are calculated with respect to the undeformed blade as shown in Fig. 5.
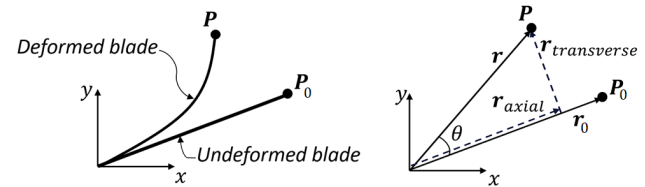

FIGURE 5. Vector diagram of axial and transverse displacement

Firstly, a study of the number of modes necessary to obtain a converged solution is conducted by using only 1 substructure divided into 22 Finite Elements. For the linear model L, a converged solution is obtained with 1 axial and 6 transverse modes as shown in Fig. 6 while the NL1 formulation needs 2 axial and 6 transverse modes to converge as shown in Fig. 7. The geometric stiffening due to axial loading increases the need for axial modes comparing the converged results of L and NL1. Nevertheless, there is no a clear convergence behaviour.

A case study of the blade model is conducted by varying the number of substructures from 1 to 12 and comparing the response of the linear formulation with the response obtained by accounting for the non-linear elastic forces. In Figures 8 and 9 the transverse and axial tip displacements are presented, respectively, using 1, 2, and 12 substructures with the linear elastic model L. By increasing the number of substructures, the transverse displacement is reduced due to a better representation of
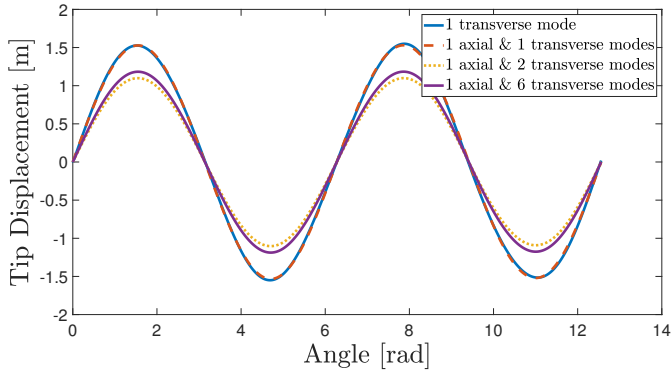
FIGURE 6. Steady state response of transverse tip displacement for Linear Model ($\omega = 1.6$ rad/s)
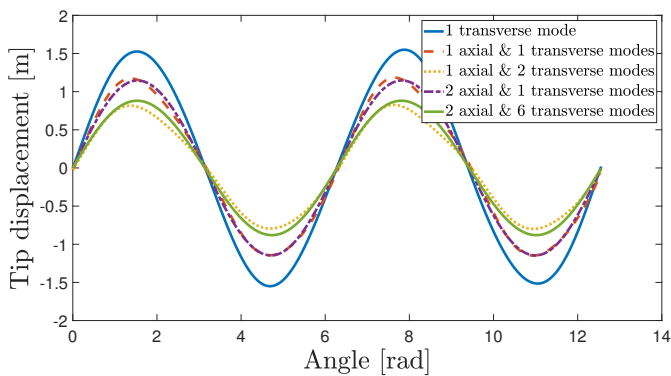

FIGURE 7. Steady state response of transverse tip displacment for Nonlinear Model 1 ($\omega = 1.6$ rad/s)
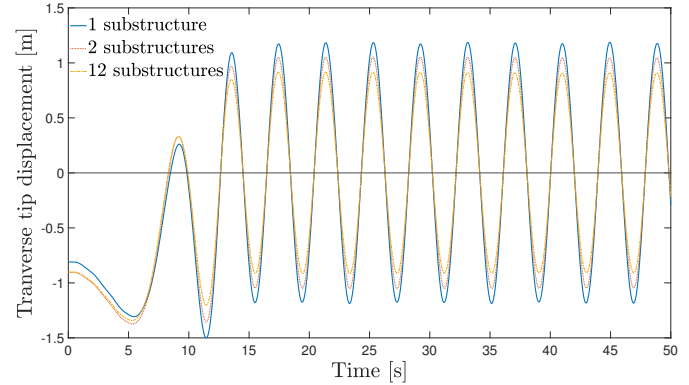

FIGURE 8. Transverse tip displacement for 1, 2, and 12 substructures using the linear elastic model (L)
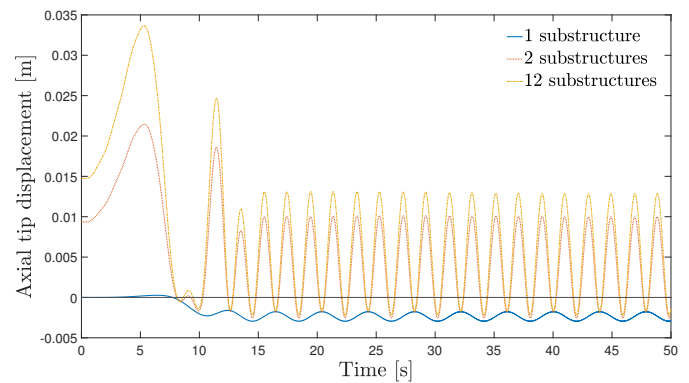
FIGURE 9. Axial tip displacement for 1, 2, and 12 substructures using the linear elastic model (L)

geometric stiffening. In the case of the axial displacement, 1 substructure predicts only negative displacement, which represents an elongation of the blade due to centrifugal forces. However, as the number of substructures increases, large displacements are correctly represented and foreshortening effect seems to occur as represented schematically in Figure 5.

Both figures show similar behaviour when varying the number of substructures, but with different predictions in peak displacement in steady-state. For the axial displacement, a significant difference is obtained when using more than one substructure, which is caused by the foreshortening effect. The effect of gravity is also observable in the axial displacement as the gravitational forces alternate between working against and with the centrifugal forces.

In Fig. 10, it is observed that the axial displacement oscillates with twice the frequency of the transverse displacements. This indicates that the foreshortening effect dominates the axial displacement, so that every time the blade is bent to the utmost position, in either direction, a maximum is reached in the axial displacement as well. Every time the transverse deflection

changes sign, the axial deflection is at a minimum and in a state of stretch, indicating that the centrifugal forces are pulling the blade in its longitudinal direction.

A comparison of the maximum axial and transverse tip displacements in steady-state between the two elastic models L and NL1 can be seen in Fig. 11 and 12. The number of substructures used has also been varied from 1 to 12.

Increasing the number of substructures stiffens the transverse displacement response for the elastic model L. In the nonlinear model (NL1), where the geometric stiffening effect is included, the response is close to the converged result using only 1 substructure. However, this is not the case for the axial displacement, where similar behaviour is observed between the two elastic models when increasing the number of substructures. Nonlinear model (NL1) is not able to improve the convergence, since it assumes that bending does not change the longitudinal position of the blade and therefore it does not account for foreshortening effect at any extent. Even more, the stiffening effect introduced by NL1 makes the axial displacement converge slower compared
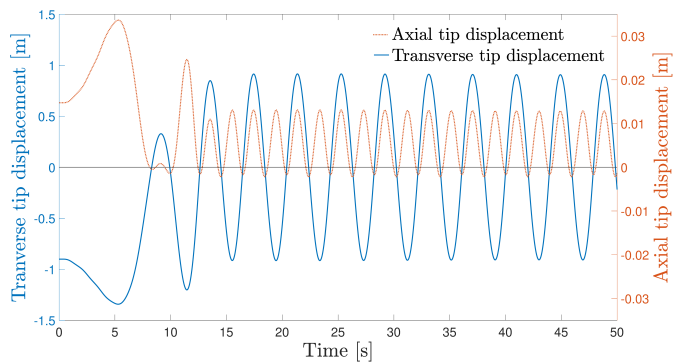
FIGURE 10. Tip displacements using the linear elastic model (L) with 12 substructures

to the linear elastic model (L) since the bending stiffness is relatively larger.

Regarding the computational cost, the linear approach is overall less expensive than NL1. For 9 substructures, the computational cost of NL1 equals that of the linear theory using 12 substructures. Therefore, despite an increased computational cost NL1 might still offer a better performance.
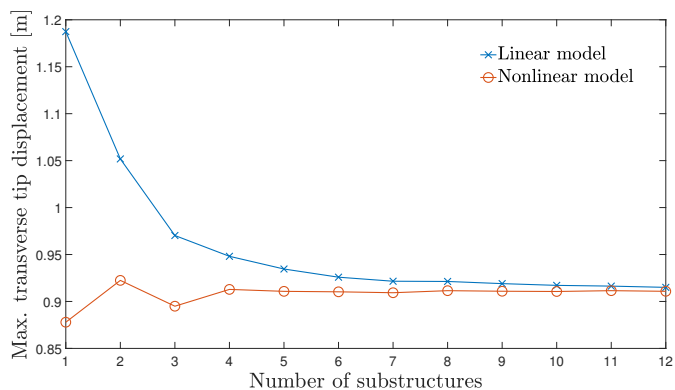

FIGURE 11. Max. transverse tip displacement in steady state for the two elastic models and varying substructures (ω=1.6 rad/s)

6 Summary and Conclusions

A 2D case study of a blade from a 2.75 MW wind turbine is conducted by modelling the blade as a non-prismatic beam based on data from a wind turbine blade. The floating frame of reference formulation is applied to model the flexibility of a wind turbine blade. The stiffness of the blade is described by a Finite Element formulation by discretizing the blade into several Euler-Bernoulli beam elements. To capture geometric nonlinearity deformations both the substructuring technique and the nonlinear
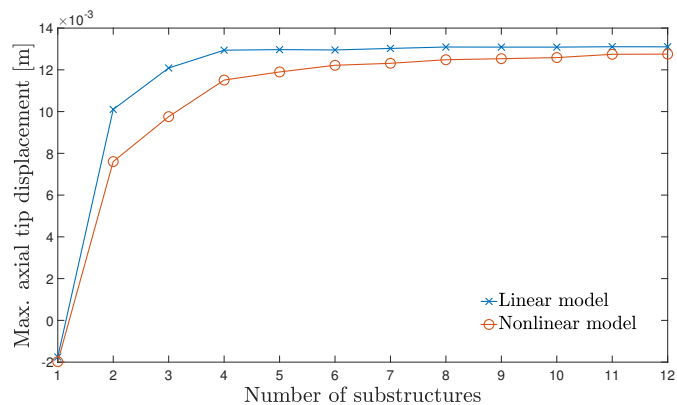

FIGURE 12. Max. axial tip displacement in steady state for the two elastic models and varying substructures (ω=1.6 rad/s)

elastic forces are applied. These methods couple the axial and transverse displacement.

The numerical results displayed in this paper demonstrate that a single substructure with a linear elastic model may not be able to represent a wind turbine blade when non-linear phenomena occur. The foreshortening effect is not captured when the blade is bent, and the transverse tip displacement is estimated too large. Increasing the number of substructures improves the blade modelling.

The nonlinear model describes the transverse tip deflection better than the linear model using fewer substructures, but a similar ability in describing the foreshortening effect is seen for the elastic models L and NL1. This is due to the bending-stretching coupling being included in the nonlinear elastic model (NL1) so that a stiffening effect is introduced. However, since transverse deflections affect more the blade and wind turbine performances in terms of loading and fatigue than axial ones, it is concluded that accounting for the contribution of nonlinear elastic forces minimizes the number of substructures necessary to achieve the convergence of the blade model.

REFERENCES

[1] NREL, 2022. *OpenFAST Documentation*.

[2] Wang, Q., Sprague, M. A., Jonkman, J., Johnson, N., and Jonkman, B., 2017. "Beamdyn: a high-fidelity wind turbine

blade solver in the fast modular framework". *Wind Energy,* *20*(8), pp. 1439–1462.

[3] Couturier, P. J., and Skjoldan, P. F., 2018. "Implementation of an advanced beam model in BHawC". *Journal of Physics: Conference Series, 1037*, jun, p. 062015.

[4] Larsen, T. J., and Hansen, A., 2021. How 2 hawc2, the user's manual. Tech. rep., DTU.

[5] Hassan, G., and Ltd, P., 2018. Bladed theory manual. Tech. rep., DNV-GL.

[6] Shabana, A. A., 2020. *Dynamics of Multibody Systems*. No. ISBN: 978-0-521-85011-2 in Fifth Edition. Cambridge.

[7] Manolas, D. I., Riziotis, V. A., and Voutsinas, S. G., 2015. "Assessing the Importance of Geometric Nonlinear Effects in the Prediction of Wind Turbine Blade Loads". *Journal of Computational and Nonlinear Dynamics, 10*(4), 07. 041008.

[8] Wu, L., Tiso, P., Tatsis, K., Chatzi, E., and van Keulen, F., 2019. "A modal derivatives enhanced rubin substructuring method for geometrically nonlinear multibody systems". *Multibody system dynamics, 45*(1), pp. 57–85.

[9] Gaertner, E., Rinker, J., Sethuraman, L., Zahle, F., Anderson, B., Barter, G., Abbas, N., Meng, F., Bortolotti, P., Skrzypinski, W., Scott, G., Feil, R., Bredmose, H., Dykes, K., Shields, M., Allen, C., and Viselli, A., 2020. Definition of the iea 15-megawatt offshore reference wind. Tech. rep., NREL.

[10] Wu, S.-C., and Haug, E. J., 1988. "Geometric non-linear substructuring for dynamics of flexible mechanical systems". *International Journal for Numerical Methods in Engineering, 26*(10), pp. 2211–2226.

[11] Gözcü, O., and Verelst, D. R., 2020. "The effects of blade structural model fidelity on wind turbine load analysis and computation time". *Wind Energy Science, 5*(2), pp. 503–517.

[12] Bortolotti, P., Tarres, H. C., Dykes, K. L., Merz, K., Sethuraman, L., Verelst, D., and Zahle, F., 2019. Iea wind tcp task 37: Systems engineering in wind energy – wp2.1 reference wind turbines, tech. rep. Tech. rep., NREL.

[13] Bak, C., Zahle, F., Bitsche, R., Kim, T., Yde, A., Henriksen, L. C., Hansen, M. H., , and Natarajan, A., 2013. The dtu 10-mw reference wind turbine. Tech. rep., DTU Wind Energy.

[14] Bakr, E., and Shabana, A. A., 1986. "Geometrically nonlinear analysis of multibody systems". *Computers & structures, 23*(6), pp. 739–751.

[15] Mayo, J., and Domínguez, J., 1997. "A finite element geometrically nonlinear dynamic formulation of flexible multibody systems using a new displacements representation". *Journal of Vibration and Acoustics, 119*, pp. 573–581.

[16] Mayo, J. M., García-Vallejo, D., and Domínguez, J., 2004. "Study of the geometric stiffening effect: comparison of different formulations". *Multibody System Dynamics,* *11*(4), pp. 321–341.

[17] Mayo, J, D. J., and Shabana, A. A., 1995. "Geometrically nonlinear formulation of beams in flexible multibody dynamics". *Journal of Vibration and Acoustics, 117*, pp. 501–509.

[18] Ghaboussi, J., Pecknold, D. A., Wu, X. S., 2019. *Nonlinear Computational Solid Mechanics*. No. ISBN: 978-0-367-87524-4 in First Edition. CRC Press: Taylor & Francis Group.

[19] Reddy, J. N., 2017. *Energy Principles and Variational Methods in Applied Mechanics*. No. ISBN: 978-1-119-08737-3 in Third Edition. New York: John Wiley Sons, Incorporated.

[20] Sharf, I., 1996. "Geometrically non-linear beam element for dynamics simulation of multubody systems". *International Journal for Numerical Methods in Engineering, 29*, pp. 763–786.

[21] Przemienieckj, J. S., 1968. *Theory of Matrix Structural Analysis*. No. ISBN: 9780486649481 in First Edition. McGraw-Hill.

[22] Holm-Jørgensen, K., and Nielsen, S. R., 2009. "A component mode synthesis algorithm for multibody dynamics of wind turbines". *Journal of Sound and Vibration, 326*(3-5), pp. 753–767.

[23] Cook, R. D., 2002. *Concepts and Applications of Finite Element Analysis*. No. ISBN: 978-0-471-35605-9 in Fourth Edition. John Wiley & Sons.